Experimental findings in 180° backscattering enhancement from solids

H. Ellmer, W. Fischer, A. Klose, and D. Semrad

Institut für Experimentalphysik, Johannes-Kepler-Universität, A-4040 Linz, Austria

(Received 25 July 1996)

We use a backscattering assembly developed recently to investigate the enhanced backscattering from polycrystalline materials near 180°. The nominal scattering angle can be continuously varied between exactly 180.0° and 178.5°. It is shown that the stochastic model of flux peaking, though its predictions are surprisingly consistent with experimental results, either does not apply to real measurements or does only take account of a negligible fraction of the effect, which cannot be documented by experiment. The energy loss of He projectiles along correlated inward and outward trajectories turns out to be the same as in any random direction. To get the enhancement factor unaffected from detector resolution we measured the integrated backscattering yield from a number of targets with different thickness and deduced the yield by two different methods. For 400 keV He projectiles scattered from partly oxidized Ta a maximum enhancement factor of 2.8 is found. [S0163-1829(97)06405-9]

I. INTRODUCTION

Investigation of solid targets by Rutherford backscattering with swift light ions at precisely 180° can provide more distinct or even additional information compared to normal backscattering. This applies especially to single crystals, where uniaxial double alignment allows one to study simultaneously both channeling and blocking in the same low index direction. The field of application of highly collimated 180° backscattering can be extended when the scattering angle of the detected projectiles can be continuously varied in the vicinity of 180°. For instance, a thorough understanding of the 180° yield enhancement[1] asks for this option. Up to now, almost all measurements in this field have been done with a detector positioned close to the incoming beam. As a matter of fact, projectiles backscattered at exactly 180.0° miss this detector. Recently, we have developed a 180° facility which allows us to continuously vary the scattering angle of detected projectiles between true 180° and 178.5°. To our knowledge, it is the only device having this virtue. By this, we have investigated the behavior around 180° of quantities related to the enhancement effect.

We want to point out that our facility also offers the possibility to investigate energy loss processes in channeling conditions[2] using backscattering geometry; one then no longer depends on the use of thin self-supported single crystals foils as is necessary in transmission experiments. The concept of this method has been published by Hetherington,[3] who measured the stopping power of InP for 2.5 MeV He ions in ⟨110⟩ and ⟨111⟩ channels. The target consisted of a cap of InP covering a thin strained layer of InAs grown on an InP substrate. The InAs layer is fully strained so that off-normal channels are bent at the interfaces. Usually, channeled projectiles can not follow the bend and are dechanneled catastrophically.[4] The strained layer acts as a marker which gives rise to the backscattering signal. Hetherington measured the energy of scattered projectiles leaving the crystal at random directions. To study the change in energy loss when going from channeling to random directions he had to swivel the target out of alignment with the beam. Hence,

information on stopping power was obtained by varying the *in-going* trajectories. The main shortcoming[5] of this procedure is that it also changes the phase of the oscillatory projectile motion at the interface. This could change the point within the strained layer at which dechanneling occurs and, hence, change the strength of the dechanneling effect; under unfavorable circumstances, the oscillating channeled beam could even follow the bend of the channel without any appreciable dechanneling (resonance channeling[4]).

To avoid this problem, one has to keep the crystal aligned with the beam, and the information on energy loss has to be obtained from projectiles following different *out-going* trajectories, in any suitable channel, on principle. However, it follows from the reversibility of trajectories that conditions which lead to strong dechanneling also feed a great number of backscattered projectiles into the same channel. Hence, an uniaxial double alignment geometry with variable scattering angle is ideally suited for stopping power measurements in crystals. With our facility we intend to study energy and electron transfer processes of He projectiles in channels.

II. EXPERIMENTAL LAYOUT

The facility is fully described in Ref. 6; here we give only a short summary of relevant details. The 180° backscattering assembly is an improved version of our first model:[7] in both cases the 180° backscattered projectiles are deflected out of the incoming beam by a vertical magnetic field. To reduce the dispersion of the magnetic field we have now added an electric field (see Fig. 1) so that the essential part of the spatially dispersed spectrum hits a 300 mm² detector [a particle implanted and passivated silicon (PIPS) detector made by ORTEC]. The detector and the input stage of the preamplifier are kept at constant temperature of 161 K by a mixture of liquid and solid CS_2, which has a melting enthalpy of 4.39 J/mol comparable to that of ice (6.01 J/mol). In spite of the large area of the detector, we obtain a resolution of 9.1 keV for 400 keV He projectiles. The detector unit is mounted on a dewar which can be moved in the vertical direction by a linear motion feedthrough.
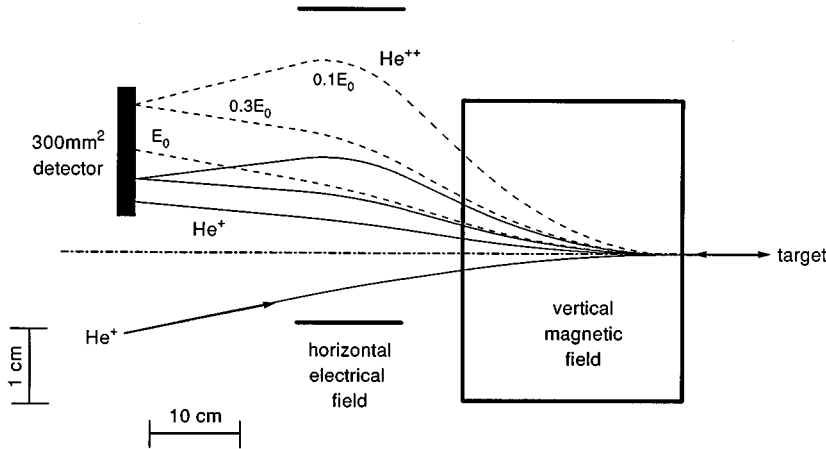
FIG. 1. Ion optics of the 180° assembly. Shown are the trajectories of He$^+$ (solid lines) and He^{++} projectiles (broken lines) backscattered with E_0, $0.3E_0$, and $0.1E_0$, where E_0 is the energy of the incoming He$^+$ projectiles. Note that the transverse scale is blown up by a factor of 10.

The 180° assembly is attached to the beam transport system of a 700 keV single ended Van de Graaff accelerator. Two baffles (B_1: $\varnothing$1.2 mm and B_2: $\varnothing$0.8 mm, 2450 mm apart) collimate the beam to a maximum incident half-angle divergence of $\alpha=0.023°$; the root mean square angle of all trajectories with respect to the beam axis is $\alpha_{rms}=0.012°$. After being deflected by the electric and magnetic fields the beam passes a vertical slit B_3 of 1.15 mm width. As the slit intercepts the rim of the beam it is made from beryllium to minimize background due to scattering. The length of the flight path between B_3 and the target is 1160 mm. The beam spot on the target is roughly elliptic (2.0×2.3 mm). In the target chamber, at a scattering angle of 170°, there is another detector which is used as fluence monitor; all spectra measured near 180° are normalized to the number of projectiles registered by this detector. The x component (in the horizontal plane) of the acceptance angle β for backscattered projectiles is given by the width of the vertical slit B_3 ($\beta_x=0.078°$). The vertical y component is exclusively determined by the detector baffle. Hence, by moving the detector and its baffle up or down, we can change this component of the backscattering angle and therefore the total backscattering angle. In addition to the scattering angle θ we have introduced the backscattering angle $\phi=180-\theta$. With the detector positioned in the plane of the incoming beam we measure projectiles scattered at a nominal backscattering angle of 0°, and with the detector shifted up by $h=52.5$ mm projectiles scattered at 1.5°. The nominal backscattering angle $\phi=0.0286h$ is the angle between beam axis and the trajectory through the center of the detector baffle. The height of the detector baffle of 3 mm determines the acceptance angle in the vertical plane, which is $\beta_y=0.078°$. For the root mean square angle we get $\beta_{rms}=0.039°$. Due to the finite emittance of the beam and to the finite acceptance of the detector, with the detector shifted up by a distance h (given in mm) we measure projectiles with a root mean square scattering angle θ_{rms} (all angles in degrees) of

$$\theta_{rms}=180°-\sqrt{(0.0286h)^2+\alpha_{rms}^2+\beta_{rms}^2}. \quad (1)$$

Hence, with the detector in the 180° position ($h=0$) the relevant rms scattering angle is 179.96°.

III. A THEORETICAL DESCRIPTION OF CORRELATION IN BACKSCATTERING EXPERIMENTS

A. Basic considerations for enhancement

We assume normal incidence in the z direction of the incoming beam on the target. The number $I(z)$ of projectiles per second backscattered into the detector from a layer at a depth z and of thickness Δz is given by

$$I(z)=\frac{d\sigma}{d\Omega}\int f(x,y;z)N(x,y;z)\Delta z\Delta\Omega_D(x,y;z)dx\,dy. \quad (2)$$

For scattering around 180° the differential scattering cross section $d\sigma/d\Omega$ is stationary and has been taken out from the integral. All other quantities apply to depth z: $f(x,y;z)$ is the flux distribution function (m^{-2} s^{-1}) and $N(x,y;z)\Delta z$ the areal atomic number density; it is given by $N(x,y;z)\Delta z=\Sigma\,\delta(x-x_j)\delta(y-y_j)$ with j running from 1 to $N_0\Delta z$, where N_0 is the average atomic number density of the target. $\Delta\Omega_D(x,y;z)$ is the local solid angle of the detector defined by all trajectories starting from position (x,y) and hitting the detector. Obviously, both $f(x,y;z)$ and $\Delta\Omega_D(x,y;z)$, depend on atoms positioned between surface and depth z. When the functions in the integral are not correlated we get the well-known equation of the product of their mean values $I_0(z)=d\sigma/d\Omega I_B N_0\Delta z\Delta\Omega_{D0}$, with $I_B=\int\int f(x,y;z)dx\,dy$ the number of incident projectiles per second and with $\Delta\Omega_{D0}$ the standard solid angle of the detector. Any correlation results in a deviation of $I(z)$ from $I_0(z)$: correlation between $f(x,y;z)$ and $N(x,y;z)$ is called channeling, correlation between $\Delta\Omega_D(x,y;z)$ and $N(x,y;z)$ is called blocking, and correlation between all three quantities, $f(x,y;z)$, $N(x,y;z)$, and $\Delta\Omega_D(x,y;z)$, is called uniaxial double alignment.

Here we will focus on correlation between $f(x,y;z)$ and $\Delta\Omega_D(x,y;z)$ with the atoms distributed at random, resulting in 180° yield enhancement. In the following, we make several simplifications, commonly used in similar discussions: momentum transfer leading to deflection of the projectile does not imply energy transfer, the target atoms stay at rest, and the electronic energy loss can be neglected. For positive projectiles, these assumptions do not severely bias the result.[1,8,9,10] Hence, projectiles scattered through 180° at a

depth z will exactly follow the inward trajectory on their way out. So we can modify Eq. (2). Within the small transverse phase space occupied by the beam, the density of particles n_0 can be assumed constant. By analogy, using Liouville's theorem we can introduce a local solid angle angle of the beam, $\Delta\Omega_B(x,y;z)$:

$$n_0 = \frac{I_B}{A_{B0}\Delta\Omega_{B0}} = \frac{f(x,y;z)}{\Delta\Omega_B(x,y;z)}. \tag{3}$$

A_{B0} is the minimum cross section of the beam (at its waist), and $\Delta\Omega_{B0}$ the solid angle as determined by baffles B_1, B_2, and B_3. By Eq. (3) we can interchange local solid angle and local flux distribution. So we finally get

$$I(z) = \frac{d\sigma}{d\Omega} N_0 \Delta z \frac{I_0}{A_{B0}\Delta\Omega_{B0}}$$
$$\times \int_A \Delta\Omega_B(x,y;z)\Delta\Omega_D(x,y;z)dx\,dy. \tag{4}$$

If we normalize to the yield expected for uncorrelated solid angles, we get the so-called enhancement factor[9] $\Gamma(z)$. Eq. (4) becomes

$$\Gamma(z) = \frac{\int_A \Delta\Omega_B(x,y;z)\Delta\Omega_D(x,y;z)dx\,dy}{A_{B0}\Delta\Omega_{B0}\Delta\Omega_{D0}}. \tag{5}$$

Γ depends on depth z and on the position of the detector relative to the beam.

Following the concept of the stochastic model presented in Ref. 11, we can split the integral in Eq. (5) into two parts:

$$\Gamma(z) = \frac{\int_A \Delta\Omega_B^2(x,y;z)dx\,dy + \int_A \Delta\Omega_B(x,y;z)[\Delta\Omega_D(x,y;z) - \Delta\Omega_B(x,y;z)]dx\,dy}{A_{B0}\Delta\Omega_{B0}\Delta\Omega_{D0}}. \tag{6}$$

In our layout $\Delta\Omega_{B0}$ is about 2.5% of $\Delta\Omega_{D0}$, so the second integral is always positive and is larger than the first by at least a factor 10. It should be stressed that in all experiments with planar detectors positioned close to the beam or with annular detectors,[1,12,13] the first integral does not contribute at all. Reference 11 only deals with the first integral. Nevertheless, it seems meaningful to distinguish between these two contributions as their relative enhancement and their depth dependence might be different. According to statistics, the first integral gives the average of the square of solid angle (or of flux) which is the sum of the square of the average, Ω_{B0}^2 and of the variance var(Ω_B). The variance is always positive except for a uniform distribution of Ω_B where it vanishes. So an increased contribution from the first integral can be directly related to an inhomogeneous flux or to flux peaking, in our diction to solid angle peaking, as described by the variance. This peaking effect is discussed in Refs. 10 and 11 on the basis of shadow cones behind target atoms and of rainbow scattering. At larger depths z, the beam is blown up in angle due to multiple scattering, so the shadow cones become obscured and rainbow scattering will be less effective. The flux gets more uniform and the variance decreases. But there will always be shadow cones so that the variance will stay positive, and a residual enhancement should survive up to large depths. When looking for reasons for differences in the intensity of the enhancement, the most prominent effect is that the first integral describes sets of interchangeable inbound and outbound trajectories. Both emerge from and merge into the beam, respectively. Therefore, projectiles can enter the target along one of both trajectories and return via the other. This is not true for the second integral as the average of the two solid angles is zero. The integral yields the sum of the product of the mean values, $\Omega_{B0}(\Omega_{D0} - \Omega_{B0})$,

and of the covariance, cov($\Omega_B,\Omega_D - \Omega_B$), which can be positive as well as negative. A negative correlation for scattering angles smaller than about 179.5° gives yield depletion[14] which has to exist for conservation of the number of scattered projectiles.

The enhancement given by the second integral is due to focusing of trajectories; if at a depth z the angle between entry and exit path is not larger than about 0.2° (in the case of 1 MeV He$^+$ onto Pt) it tends to get even smaller when the backscattered projectile leaves the target.[15,16] Obviously, there is some correlation between the scattering processes along the way into and out of the target, which can be quantified by a so-called similarity factor.[10] This correlation will get lost due to close encounters where a small difference in impact parameter results in a large difference in scattering angle, so that neighboring trajectories become separated and will penetrate different regions of the target. As in the two-atom model,[14] the decreasing enhancement with increasing depth may be elucidated by the exponentially decreasing probability $\exp(-N_0 r_0^2 \pi z)$ that there is no encounter with an impact parameter smaller than some critical value,[15] e.g., the Thomas-Fermi screening length r_0. From this one may conclude that this contribution should extend to much shallower depths than that given by the first integral.

In summary, we may say that the existence of interchangeable trajectories according to the stochastic model in contrast to the correlation of trajectories may lead to a larger enhancement which may also extend to larger depths. Therefore, we have investigated the enhancement in the vicinity of 180°, especially in the transient region where the overlap of the solid angles of detector and beam goes from its maximum value between $h=0$ and $h=1$ down to zero at $h=2$ (see Sec. III B). Furthermore, we have tried to find a difference in
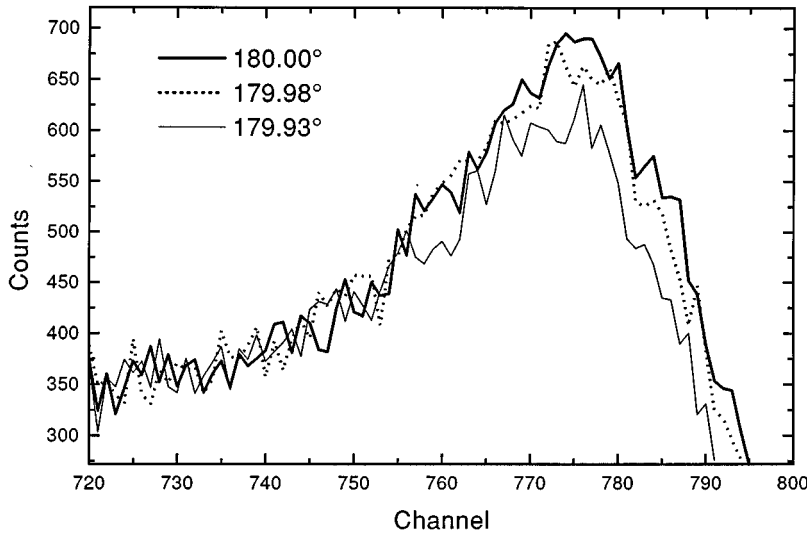
FIG. 2. Spectra of 400 keV He projectiles backscattered from a thick gold target. The nominal scattering angle is (a) 180°, (b) 179.98°, and (c) 179.93°. The dispersion of the detector system is 0.44 keV/channel.

energy loss of projectiles scattered closely to 180° compared to projectiles scattered at angles smaller than 179.5°. It was suggested[17] that due to the absence of close encounters with the target nuclei on their way through the target these particles may have more bound electrons and hence suffer less energy loss. In Sec. III C we present measurements of the true depth dependence of the enhancement unaffected by the finite detector resolution.

B. Measurement of the angular dependence of enhancement

To obtain a large enhancement, one should provide for optimum conditions for reversibility of trajectories. The projectile has to be much lighter than the target atom to keep elastic energy loss in the backscattering event small.[8] For projectiles backscattered from depths z relevant for enhancement, the time T from entrance until exit has to be small, so that the distribution of target atoms remains essentially constant. Here, it is useful to introduce the relation for depth scaling based upon the two-atom model by Oen[14]

$$N_0 Z_1 Z_2 z^2 / E_1 = \text{const}, \tag{7}$$

where N_0 is the atomic density and Z_1 and Z_2 are the charge numbers of projectile and target, respectively. E_1 is the projectile energy. Qualitatively, this scaling has been confirmed by experiment:[13] with increasing energy, the maximum enhancement is shifted to larger depths, and this holds also for targets with smaller atomic density. Introducing $E_1 = m_1 v_1^2 / 2$ and $z/v_1 \approx T/2$, we get

$$N_0 (Z_1 / 2 m_1) Z_2 T^2 = \text{const} \tag{7a}$$

and we see that T does not depend upon projectile energy. To obtain small T, we should choose a target with large charge number and high atomic density. Although Eq. (7a) favors protons above all other projectiles, we choose helium projectiles in view of our planned stopping power measurements. We still have to select the projectile energy. To get a large enhancement factor Γ, E_1 should be small.[9] For energies below the stopping power maximum, this will also reduce inelastic energy loss. Therefore, all measurements have

been performed with 400 keV He ions; here, the target was a thick layer of Au evaporated onto a silicon wafer.

Since all the spectra taken with the 180° detector were normalized to the integrated spectrum of the 170° detector, they all refer to the same fluence. For calibration purposes one can take advantage of the fact that the yield enhancement is limited[12] to angles θ larger than 179.4° and to target depths less than 70 nm. Hence, the enhancement factor can be derived from the ratio of a particular normalized spectrum to that at 178.5°. In their low-energy regions (corresponding to backscattering from depths larger than 70 nm) both spectra have to coincide, provided the width of baffle B_3 and hence the acceptance of the detector does not depend on height h. Indeed we have found that the baffle width stays constant within 3%.

In Fig. 2 we show three backscattering spectra obtained with the detector at (a) $\theta = 180.00°$ ($h=0$, $\theta_{rms}=179.96°$), (b) $\theta = 179.98°$ ($h=0.8$, $\theta_{rms}=179.95°$), and (c) $\theta=179.93°$ ($h=2.5$, $\theta_{rms}=179.92°$). We want remind the reader that the first two spectra include a contribution from the first integral in Eq. (6), but not the third. Obviously, there is no dramatic change in the shape of the spectra when going from (b) to (c) ($\Delta\theta_{rms}=0.03°$) as compared to going from (a) to (b) ($\Delta\theta_{rms}=0.01°$). All three spectra coincide in the region below channel 760, where enhancement is still present; a different depth dependence due to flux peaking is not discernible.

To describe the yield enhancement in a quantitative way, we have chosen the areal number density of excess atoms[9] which would give the same additional yield. This quantity is sensitive both to the magnitude of the effect and to its extension in depth. In Fig. 3 we show N_{excess} as a function of the nominal backscattering angle. The spline fit is to guide the eye. Again, we get a smooth function. This is an indication of a smooth transition between variance [described by the first integral in Eq. (6)] and covariance (described by the second integral). Also the fact that the prediction of the stochastic model[11] is consistent with measurements using a planar detector positioned close to the incoming beam points this way: this model should not be applicable at all. Though no real experiment meets the requirements to be (exclu-
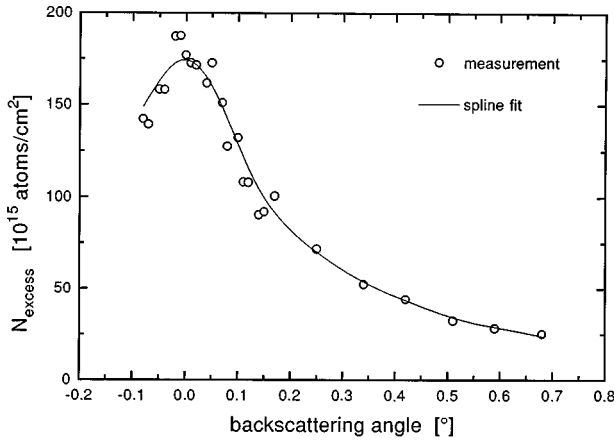
FIG. 3. Number of excess atoms per unit area which will give the same measured yield enhancement as function of nominal backscattering angle. 400 keV He ions hit a massive gold target. The spline fit is to guide the eyes.

sively) described by the stochastic model, it gives a good estimate of the 180° yield enhancement. Obviously, flux peaking not only results in an increase of the variance (which is the base of the stochastic model) but also in an increased probability for correlated inward and outward trajectories. This is confirmed by calculations with a Monte Carlo program which show that the depth dependence of the inhomogeneity of the flux distribution perfectly pictures that of the yield enhancement.

The spline fit to the data in Fig. 3 show a peak centered at $\theta = 180°$, with a full width at half maximum angle of 0.36°, and a long tail extending beyond a backscattering angle of 0.8°. This behavior can be understood in the light of the discussions in Refs. 8 and 15. For shallow depth, there is a modest enhancement at small angles but with a large width followed by a yield deficit at even larger angles. Advancing in depth, the enhancement will become more pronounced but both the angular width of the enhancement and the angular position of the deficit will move inward. Only at 180° we will find a constructive superposition from all depths. Considering enhancement as a function of angle, contributions from larger depths get lost or even reduce the effect with increasing angle. So we expect a cusplike shape. Actually, due to the finite acceptance angle of the detector the tip of the cusp is flattened.

We have also compared the specific energy loss of 400 keV helium projectiles with correlated inbound and outbound trajectories with that of random particles. For this purpose we used polished Si single-crystal backings covered first with a thick film of Al and then with a thin Ta marker and a layer of Cu (between 10 and 20 nm thick). The backscattering spectrum shows the peaks of Ta and Cu followed at lower energies by the broad spectra of the Al film and of the Si backing. By comparing the area of the Cu peak to the height of the Al spectrum we can estimate[18] the areal mass density of the top Cu layer. To find any difference in energy loss we have to look for a shift of the Ta peak when varying the backscattering angle from 180° to 178.5°. We did not find any effect within an uncertainty of about 0.4 keV, which is 2–4 % of the total energy loss of 400 keV He ions traversing the Cu layer twice. So we can state that projectiles

guided forth and back in some sort of ``wells with no atoms of the solid within a few tens of pm''[11] suffer the same energy loss as in any random direction, within 4%.

C. Measurement of the depth dependence of enhancement

Here, we are interested in the normalized yield enhancement factor as a function of depth

$$\Gamma(z) = \frac{Y_{180}(z)}{Y_{178.5}(z)}, \tag{8}$$

where $Y_{180}(z)$ and $Y_{178.5}(z)$ are the number of projectiles backscattered at a depth z from a layer of thickness Δz and exiting the target at an angle close to 180° and to 178.5°, respectively. As shown above, depth scale can be converted to energy scale and vice versa by using random stopping power values, so we get $N(E) = Y_{180}(E)/Y_{178.5}(E)$. Energy E is related to depth z by (Ref. 18) $E = kE_0 - (S)z$, where E_0 is the beam energy and (S) is the stopping power factor. Unfortunately, only the yields convoluted with the detector resolution $G(E',E)$ are accessible to experiment:

$$\Gamma_{\text{exp}}(E') = \frac{\int Y_{180}(E)G(E',E)dE}{\int Y_{178.5}(E)G(E',E)dE}. \tag{9}$$

In the region of the maximum, Γ_{exp} is considerably smaller than Γ but, unfortunately, only data for $\Gamma_{\text{exp}}(E')$ have been published until now. Clearly, one needs some sort of resolution correction to obtain Γ. As we showed in Ref. 19, only parametrization of the problem will give satisfying results, and only if a function dependent on a small number of parameters can be found which properly describes $Y(E)$.

But since we were not able to find a suitable function, we measured the integral yield $Z(z) = \int_0^z Y(\zeta)d\zeta$ instead, to avoid resolution problems. Here, we again consider Y a function of z. $Z(z)$ is the total number of projectiles backscattered from a layer of thickness z and is therefore unaffected by detector resolution. We can make use of $Z(z)$ twice, as follows: when we take the difference ΔZ for two targets of nearly equal thickness, we get $\Delta Z = \bar{Y}\Delta z$, where $\bar{Y}$ is the yield averaged over the difference in target thickness Δz. In contrast to the measurement of N_{exp}, where $Y(z)$ is averaged over the depth resolution of the detector, we can make Δz arbitrarily small, in principle.

Alternatively, we may take ratios instead of differences, introducing the ratio of integrated yields, Ξ_{exp}:

$$\Xi_{\text{exp}}(z) = \frac{Z_{180}(z)}{Z_{178.5}(z)} = \frac{\int_0^z Y_{180}(\xi)d\xi}{\int_0^z Y_{178.5}(\xi)d\xi}. \tag{10}$$

If we assume that the spectrum taken at 178.5° is fairly constant for shallow depths, we can approximate the denominator by $Y_{178.5}(0)z$. When we differentiate Eq. (10) we get

$$\frac{d\Xi_{\text{exp}}(z)}{dz} = \frac{Y_{180}(z)}{Y_{178.5}(0)z} - \frac{\int_0^z Y_{180}(z)dz}{Y_{178.5}(0)z^2} = \frac{\Gamma(z)}{z} - \frac{\Xi_{\text{exp}}(z)}{z}. \tag{11}$$

Finally, $\Gamma(z)$ follows from

$$\Gamma(z) = \Xi_{\text{exp}}(z) + z\frac{d\Xi_{\text{exp}}(z)}{dz}. \tag{12}$$

We note that $\Gamma(z)$ and $\Xi_{exp}(z)$ intersect at the maximum of $\Xi_{exp}(z)$.

For the measurement, we used both methods. To obtain $\Xi_{exp}(z)$ for a large number of z values, 13 targets with thickness ranging from 3.1 to 44.4 $\mu g/cm^2$ were produced. To obtain homogeneous films even for the thinnest targets, one has to make sure that the material has negligible mobility across the substrate surface, since 180° yield measurements are very sensitive to target inhomogeneities. We selected Ta as target material. First a thick Al film was evaporated onto a polished Si single-crystal backing which was then covered by the Ta layer. By comparing the height of the Al spectrum to the area of the Ta peak, we get the areal density of Ta atoms. Determining the actual composition of our targets, we found that this corresponded roughly to Ta_4O_3. For energy-to-depth conversion we assumed Bragg's rule to be valid, and we used the stopping power from Ref. 20.

To save time, we actually did not measure the backscattering spectra at 178.5° but used the spectrum registered simultaneously by the 170° detector positioned close to the target. The better counting statistics makes up for the inaccuracy in the transformation. The peak area $A_{178.5}$ is related to the peak area A_{170} by

$$A_{178.5} = A_{170} \frac{(d\sigma/d\Omega)_{178.5}}{(d\sigma/d\Omega)_{170}} \frac{\Delta\Omega_{178.5}}{\Delta\Omega_{170}}. \quad (13)$$

The angular dependence of the scattering cross section $d\sigma/d\Omega$ is assumed to follow the Rutherford cross section. The relevant ratio of solid angles was determined separately according to Eq. (13): we obtained $\Delta\Omega_{170}/\Delta\Omega_{178.5} = 16.3 \pm 0.75$ in agreement with a geometrical determination.

The result of our measurement, $\Xi_{exp}(z)$, is presented in Fig. 4. The broken line is a spline fit to the measured data. Using Eq. (12), we get the true enhancement factor Γ as a function of depth (solid curve). As required by Eq. (12), both curves intersect at the maximum of $\Xi_{exp}(z)$.

For comparison, we also show some representative data points obtained from differences ΔZ. Here, we have to keep the interval of averaging, Δz, small, and hence, we have to accept large errors of the data which are differences of numbers comparable in magnitude. Evidently, these points confirm the solid curve. The maximum true enhancement factor of 2.8 is found for a depth of 7.3 $\mu g/cm^2$, which corresponds to 5.3 nm assuming a density of the oxidized Ta of 13.9 g/cm^3. Due to the finite detector resolution, the experimental maximum is only $\Gamma_{exp} = 2.0$.
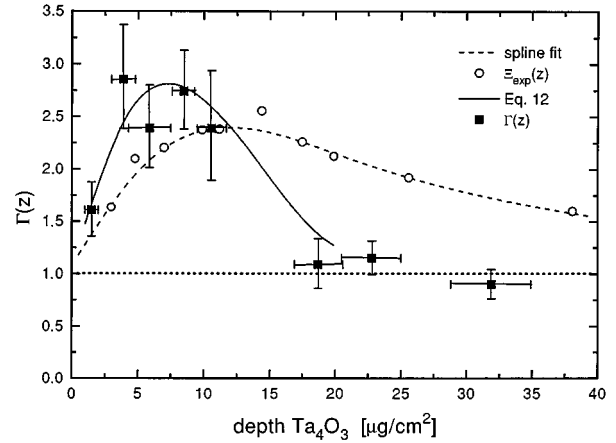
FIG. 4. The enhancement factor $\Gamma(z)$ as function of target depth for a Ta_4O_3 target. Shown are the ratios $\Xi_{exp}(z)$ of integrated yields (open symbols) measured for a number of targets of thickness z at 180° and at 178.5°, respectively. The broken curve is a spline fit to the data. The solid line gives $\Gamma(z)$ as obtained from the spline fit using Eq. (12). The data points (solid symbols with error bars) are obtained from differences of integrated yields from targets neighboring in thickness.

We have shown that the absence of close encounters of He projectiles with target atoms as is the basic requirement for correlated inward and outward trajectories leading to yield enhancement does not change the specific energy loss and hence the charge state of the projectile. Furthermore, the stochastic model describes only a small fraction of the enhancement effect measured in real experiments. But as it is based upon the occurrence of flux peaking, which seems also to be the source of increased probability for correlated inward and outward trajectories, its predictions are consistent with experimental data. Finally, we have presented a procedure to determine the true enhancement factor unaffected from detector resolution. The value of $\Gamma = 2.8$ is the largest enhancement factor determined by experiment.

ACKNOWLEDGMENTS

[1] P. P. Pronko, B. R. Appleton, O. W. Holland, and S. H. Wilson, Phys. Rev. Lett. **43**, 779 (1979).

[2] N. M. Kabatchnik, Nucl. Instrum. Methods Phys. Res. B **115**, 292 (1996).

[3] D. W. Hetherington, Nucl. Instrum. Methods Phys. Res. B **90**, 84 (1994).

[4] S. T. Picraux, W. K. Chu, W. R. Allen, and J. A. Ellison, Nucl. Instrum. Methods Phys. Res. B **15**, 306 (1986).

[5] D. W. Hetherington, Nucl. Instrum. Methods Phys. Res. B. **115**, 319 (1996).

[6] H. Ellmer, W. Fischer, A. Klose, and D. Semrad, Rev. Sci. Instrum. **67**, 1794 (1996).

[7] D. Semrad, H. Aigner, R. Golser, and P. Roth, Nucl. Instrum. Methods **205**, 287 (1983).

[8] J. H. Barrett, B. R. Appleton, and O. W. Holland, Phys. Rev. B **22**, 4180 (1980).

[9] T. E. Jackman, J. A. Davies, W. Eckstein, and J. A. Mooore, Nucl. Instrum. Methods **191**, 527 (1981).

[10] J. H. Barrett, O. S. Oen, and O. W. Holland, Phys. Rev. B **43**, 2471 (1991).

[11] O. W. Holland and J. H. Barrett, Phys. Rev. B **35**, 6495 (1987).

[12] P. P. Pronko, B. R. Appleton, O. W. Holland, and S. R. Wilson, Nucl. Instrum. Methods **170**, 227 (1980).

[13] B. R. Appleton, O. W. Holland, and J. H. Barrett, Nucl. Instrum. Methods **191**, 507 (1981).

[14] O. S. Oen, Nucl. Instrum. Methods **194**, 87 (1982).

[15] O. H. Crawford, Phys. Rev. Lett. **44**, 185 (1980).

[16] M. M. Jakas and R. A. Baragiola, Phys. Rev. Lett. **44**, 424 (1980).

[17] D. W. Mingay and B. Rosner, Nucl. Instrum. Methods Phys. Res. B **2**, 340 (1984).

[18] W. K. Chu, J. W. Mayer, and M. A. Nicolet, *Backscattering Spectroscopy* (Academic, New York, 1978).

[19] H. Ellmer and D. Semrad, Phys. Rev. E **54**, 3569 (1996).

[20] J. F. Ziegler, *Helium-Stopping Powers and Ranges in All Elements* (Pergamon, New York, 1977), Vol. 4.